
A Queuing-Theoretic Framework for Stability Analysis of LLM Inference with KV Cache Memory Constraints

Chengyi Nie¹ Nian Si² Zijie Zhou²

Abstract

The rapid adoption of large language models (LLMs) has created significant challenges for efficient inference at scale. Unlike traditional workloads, LLM inference is constrained by both computation and the memory overhead of key-value (KV) caching, which accelerates decoding but quickly exhausts GPU memory. In this paper, we introduce the first queuing-theoretic framework that explicitly incorporates both computation and GPU memory constraints into the analysis of LLM inference. Based on this framework, we derive rigorous stability and instability conditions that determine whether an LLM inference service can sustain incoming demand without unbounded queue growth. This result offers a powerful tool for system deployment, potentially addressing the core challenge of GPU provisioning. By combining an estimated request arrival rate with our derived stable service rate, operators can calculate the necessary cluster size to avoid both costly over-purchasing and performance-violating under-provisioning. We further validate our theoretical predictions through extensive experiments in real GPU production environments. Our results show that the predicted stability conditions are highly accurate, with deviations typically within 10%.

1. Introduction

Since the public release of ChatGPT in late 2022, the world has witnessed the rapid rise and widespread adoption of generative artificial intelligence (AI), particularly large language models (LLMs) (Brown et al., 2020; Chowdhery et al.,

¹Department of Electrical and Computer Engineering, Stony Brook University ²Department of Industrial Engineering and Decision Analytics, HKUST. Correspondence to: Zijie Zhou <jerryzhou@ust.hk>.

2023; OpenAI, 2023; Kaplan et al., 2020; Wei et al., 2022). These models have quickly become embedded in everyday workflows across education, business, entertainment, and research (OpenAI, 2019; GitHub, 2021; Huang et al., 2025). Recent reports (GilPress, 2024; Gordon, 2024) suggest that billions of user interactions have already taken place through LLM-powered applications. While the deployment of LLMs has substantially improved human productivity, this surge in demand also creates unprecedented challenges in reliably and efficiently serving LLM inference at scale.

At the heart of this challenge lies the process of LLM inference—the computation by which a pre-trained LLM receives input prompts and generates output tokens sequentially. Unlike traditional machine learning models, LLMs often require massive computational resources, long response times, and intricate scheduling of GPU clusters. The inherently sequential generation of tokens exacerbates these issues, as each step depends on the model’s state from the previous step. Thus, efficient inference is not merely a matter of computational optimization, but also one of system-level design to balance responsiveness, throughput, and resource costs.

A central difficulty in this design problem is understanding and ensuring the stability of LLM inference under queuing dynamics. From a systems perspective, an inference service can be modeled as a queueing network where user requests arrive randomly, wait for GPU allocation, and are processed token by token. If the arrival rate of requests exceeds the system’s effective service rate, queues will grow unbounded and the service will become unstable, leading to unacceptable latency and degraded user experience. Consequently, it is crucial to estimate the throughput and stability conditions of LLM inference in advance. Accurate estimation enables practitioners to (i) provision the appropriate number of GPUs to meet anticipated demand, (ii) design scheduling algorithms that minimize latency while maximizing utilization, and (iii) develop adaptive scaling strategies that respond to fluctuating workloads in real time.

In modern LLM inference, a crucial technique for improving efficiency is the use of the key-value (KV) cache (Pope et al., 2023; Kwon et al., 2023). During the process of the LLM inference, instead of recomputing the query, key, and

value representations for all previously generated tokens at every step, the model stores the key and value vectors in memory and reuses them for subsequent computations. This mechanism reduces the per-token computational cost of decoding from scaling with the sequence length to scaling only with the new token, thereby greatly accelerating inference. However, this acceleration comes at the expense of substantial GPU memory consumption, since the cache must retain the representations for all tokens in the active context. For requests with long prompts or long generations, the memory footprint can quickly become a bottleneck, often dominating system capacity constraints.

This memory–computation tradeoff introduces unique challenges for queueing-based modeling of LLM inference. Traditional queueing models focus primarily on computation as the limiting resource, but in LLM serving systems, both GPU compute throughput and memory availability jointly determine stability. Therefore, queueing models for LLM inference must explicitly account for the interplay between computation and memory constraints, requiring new formulations that go beyond classical service-rate abstractions.

In this paper, we develop a queueing-theoretic framework that explicitly incorporates KV cache and memory constraints into the analysis of LLM inference. To the best of our knowledge, this is the first queueing model that captures the memory dimension of GPU-based inference, which has emerged as a critical bottleneck in large-scale LLM serving. Our main contributions are threefold:

1. **Modeling.** We introduce a queueing-theoretic model for LLM inference that explicitly incorporates both computational demand and GPU memory constraints, the latter governed by the Key-Value (KV) cache. It generalizes the queueing LLM inference model in (Li et al., 2025) by adding memory awareness and refines (Jaillet et al., 2025) by reformulating its scheduling setup into a queueing framework with a chunked prefill stage. This enables a more realistic characterization of system behavior under varying prompt lengths, output lengths, and request arrival patterns.
2. **Theoretical Analysis.** Building on this model, we derive rigorous stability and instability conditions for LLM inference systems. These results provide a principled foundation for determining when a serving system can reliably handle incoming workloads, and when unbounded queue growth or system failures may occur.
3. **Empirical Validation.** We conduct extensive experiments in real GPU production environments, evaluating both single-GPU and multi-GPU configurations. Our results demonstrate that the derived stability conditions are highly accurate in practice, with prediction errors typically within 10%. These findings confirm

the practical relevance of our model and highlight its potential for guiding system design and resource provisioning.

The remainder of the paper is organized as follows. Section 2 surveys the relevant literature on stochastic bin packing problems and LLM inference. In Section 3, we present our queueing model for LLM inference. The stability conditions for LLM inference under memory constraints are derived in Section 4. Section 5 presents real GPU experiments that validate our theoretical results. Finally, we conclude the paper and discuss limitations and directions for future work in Section 6.

2. Literature Review

Queueing and LLM Inference. Recent work has begun to view large language model (LLM) inference through the lens of queueing theory. Wu et al. (2023) address the system-level challenge of serving LLMs under strict latency requirements by introducing token-level preemptive scheduling and a skip-join multi-level feedback queue. While their approach is inspired by queueing theory, it does not provide a precise queueing model or theoretical analysis. Complementing this, Yang et al. (2024) develop queueing-theoretic models to analyze the impact of stochastic output token lengths and batching policies, showing that strategies such as token clipping and elastic batching can be quantitatively optimized to balance throughput and delay. Furthermore, Li et al. (2025) study throughput-optimal scheduling algorithms and stability conditions. Guldogan et al. (2024) study the multi-bin batching strategy also from a queueing perspective. However, all of these works do not explicitly model memory constraints or the KV cache, which can lead to substantial errors in scenarios where memory is a tight bottleneck. At a broader level, Mitzenmacher & Shahout (2025) survey the intersection of queueing, prediction, and LLM-specific constraints, highlighting open problems such as robust scheduling with noisy predictions, incorporating memory footprints into queueing models, and reconciling throughput–latency tradeoffs.

Theoretical Modeling for LLM Inference. A parallel line of theoretical work focuses on scheduling algorithms for LLM inference (Jaillet et al., 2025; Ao et al., 2025; Chen et al., 2025; Wang et al., 2025; Chen et al., 2026). These studies typically model LLM inference as a resource-allocation problem in Operations Research. While our goal is to characterize the fundamental stability limit (i.e., the maximum processing rate of a given system) under stochastic prompt arrivals, prior scheduling work primarily focuses on designing policies to improve system efficiency, without deriving closed-form characterizations and without validation on real GPU systems.

Stochastic Bin Packing Problems. LLM inference with memory constraints is similar to stochastic bin packing problems, or equivalently, queueing systems with packing constraints, which have been well-studied in the literature. In stochastic bin packing problems, each request with a given bandwidth arrives online in a stochastic manner. The system manager must develop scheduling algorithms to serve the requests while satisfying the total bandwidth constraints. This problem was first modeled in [Coffman & Stolyar \(2001\)](#). [Gamarnik \(2004\)](#) then derived the stability conditions for this model under the Best-Fit scheduling policy, where the largest requests are allocated first, followed by the next largest, and so on. Subsequently, [Maguluri et al. \(2012\)](#) later generalized the model beyond additive bandwidth settings to more general configurations, studying the allocation of virtual machines to physical computers and showing that the Best-Fit algorithm is generally not throughput-optimal. [Stolyar \(2013\)](#); [Stolyar & Zhong \(2013; 2015\)](#) considered the infinite-server version of this problem, where the goal is to minimize the number of servers used. Furthermore, [Ghaderi et al. \(2014\)](#) proposed a randomized Best-Fit algorithm in this context, and [Gupta & Radovanovic \(2015\)](#) generalized the problem to cases where requests may renege and servers may slow down.

There are several key differences between stochastic bin packing problems and LLM inference with memory constraints. First, the memory footprint of a request is not a fixed count but evolves approximately linearly as processing progresses. Second, LLM inference consists of two distinct phases—the prompt phase and the token generation (decode) phase—with different memory dynamics. Third, the total available memory is typically much larger than the memory requirement of a single request, which naturally places the problem in a large-memory regime.

3. Model

To model the LLM inference process, we formulate a queueing and batching problem for a single computational worker (GPU) operating over the interval $[0, +\infty)$. The worker is subject to a KV cache memory constraint $M > 0$. We normalize the KV cache unit from bytes to tokens.

Prompt requests arrive sequentially over time, with their arrivals following a stochastic process, which we shall specify later. Let \mathcal{I} represent the instance consisting of all prompt requests within the finite time horizon. Each prompt request i has a size $s_i > 0$, defined as the number of tokens in the prompt. Additionally, each request i is associated with a response length $o_i > 0$, representing the number of tokens in the response from autoregressive LLMs. We assume that $\{s_i, o_i\}$ is independently sampled from a joint distribution $\mathcal{F}_{\text{in-out}}$ with the joint probability mass function of the number of tokens in the prompt and the corresponding response

length denoted as $p(s, o)$.

In practice, a system designer selects hardware with a memory capacity M that is significantly larger than the typical request size $(s_i + o_i)$ under the distribution $\mathcal{F}_{\text{in-out}}$. This enables high concurrency by allowing multiple requests to be processed simultaneously. Therefore, we focus on the regime where the memory requirement of a single prompt is much smaller compared with the GPU’s memory capacity, i.e., $\text{ess sup}_{s, o \sim \mathcal{F}_{\text{in-out}}} \{s + o\} \ll M$.

Prompt Processing. Each prompt request is processed online and undergoes two primary phases on the GPU worker:

1. *Prompt Phase:* Following a widely adopted approach ([Agrawal et al., 2024](#); [Ratner et al., 2022](#); [Yen et al., 2024](#); [An et al., 2024](#)), we assume that input prompts are divided into equally sized small chunks. We assume that each chunk contains \hat{s} number of tokens. Therefore, each prompt will be split into s_i/\hat{s} number of chunks¹. These chunks are processed sequentially. During this phase, the memory required for processing the j th chunk of prompt i is $j \times \hat{s}$, meaning memory usage gradually increases as the prompt is processed. When the final chunk is processed, the total memory occupied in the KV cache for prompt i reaches s_i . Once the prompt is fully processed, the model generates its first output token.

2. *Decode Phase:* After the prompt phase, subsequent tokens are generated sequentially. In this phase, the memory required for processing the j th token of prompt i ($j \in [o_i]$) is $s_i + j$. This increase occurs because each new token adds its key and value to the KV cache, contributing additional usages of memory. Consequently, by the time the final token of prompt i is processed, the total memory usage reaches $s_i + o_i$. After generating the last token, the KV cache memory allocated to prompt i is fully released.

Mixed Batching. A mixed batch may contain any unprocessed prompt chunk or output token from different requests ([Agrawal et al., 2023; 2024](#)). When a prompt chunk is added to a batch, its next chunk is generated after processing, and if it is the final chunk, the first output token is produced once the batch completes. Similarly, when an output token is included in a batch, the next token is generated upon batch completion.

In LLM services, exceeding the KV cache limit in both the GPU and the CPU causes the system to stop working. The batching constraint ensures that the total memory usage at any time does not exceed M , considering all ongoing prompt requests (i.e., those still being processed or awaiting final output tokens). Formally, let $S^{(t)}$ denote the set of prompts that have been processed but still have pending out-

¹To simplify the analysis, we assume that s_i/\hat{s} is a positive integer for all i .

put tokens at the end of time t . For each $i \in S^{(t)}$, define $c_i^{(t)}$ as the index of prefill chunk of request i having processed at the end of time t , where $c_i^{(t)} \in \{1, 2, \dots, s_i/\hat{s}\}$, and define $d_i^{(t)}$ as the index of output token of request i having processed at the end of time t , where $d_i^{(t)} \in \{0, 1, \dots, o_i\}$. Therefore, if $c_i^{(t)} < s_i/\hat{s}$, the index of output token will always be zero, i.e., $d_i^{(t)} = 0$. The memory constraint requires that, for all $t \in [0, +\infty)$, at the end of period t , the total memory usage must satisfy

$$\sum_{i \in S^{(t)}} c_i^{(t)} \hat{s} + d_i^{(t)} \leq M.$$

Work-conserving Scheduling and Continuous Batching.

In this work, we consider continuous batching. We also allow any work-conserving scheduling policy, meaning the server processes the next-priority prompt whenever it has available capacity. Examples include first-come-first-served (FCFS), as in vLLM (Kwon et al., 2023) with SARATHI (Agrawal et al., 2024), and other disciplines such as Shortest Job First (SJF).

To rigorously define the work-conserving scheduling and the continuous batching in mathematics, we consider at any $t \in [0, T]$, the policy prioritizes all ongoing processing requests and then admits new prompts into the batch according to a specified priority rule. Specifically, a new prompt is added whenever doing so does not violate the memory constraint. If, at a later time, the growing KV cache is about to exceed this constraint, the system can swap the KV cache of some prompts to the CPU at no additional cost. In practice, such swapping is rare. For example, in the vLLM implementation, GPU memory utilization is capped below one (`gpu_memory_utilization=0.9` by default).² We set M to this effective memory limit; consequently, small fluctuations above M do not immediately trigger swapping, making such SJF events infrequent in practice.

Batch Processing Time and Arrival Rates. We normalize batch processing time to one unit of time in our model, with one unit corresponding to \bar{b} seconds. Service decisions are thus made at discrete time slots. We assume that the number of arrivals in each time slot is independent across slots with rate λ , i.e., the mean number of arrivals per slot is $\lambda \bar{b}$. We now justify why this constant-time assumption is appropriate for stability analysis.

The key observation is that stability analysis focuses on the regime in which the system operates near capacity, that is, when memory utilization approaches M . In this regime, the

²https://github.com/vllm-project/vllm/blob/54a66e5fee4a1ea62f1e4c79a078b20668e408c6/vllm/engine/arg_utils.py

dominant per-batch computational cost is the attention operation, rather than memory I/O, which is bounded by memory bandwidth. When the total KV cache usage satisfies $\sum_{i \in S^{(t)}} (c_i^{(t)} \hat{s} + d_i^{(t)}) \approx M$, the total attention computation per batch becomes approximately constant (Pope et al., 2023; Kaplan et al., 2020; Hoffmann et al., 2022). Moreover, our chunked prefill formulation bounds the per-batch prefill cost by fixing the chunk size \hat{s} , thereby preventing the quadratic attention complexity of long prompts from inducing large variance. Real-world traces corroborate this behavior: over 80% of batches exhibit nearly identical processing times (see Figure 1 and Appendix B).

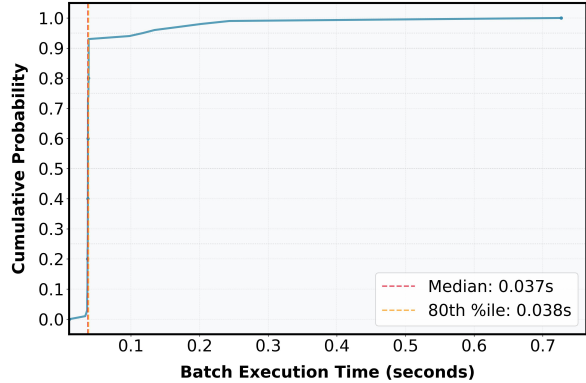


Figure 1. Cumulative Distribution Function for Batch Execution Time with PD ratio 1:1 requests

System Stability. At each discrete time step, we represent the system state by the set of prompts that have arrived but are not yet completed, $S^{(t)} \cup W^{(t)}$, along with the indices of the prefill chunk and output token processed for each request $i \in S^{(t)} \cup W^{(t)}$ at the end of time t , denoted by $\{c_i^t, d_i^t\}$. Here, $W^{(t)}$ denotes the set of prompts that have arrived but have not yet started processing at time t , where $c_i^t = d_i^t = 0$ for $i \in W^{(t)}$. This induces a countable-state, discrete-time Markov chain. For simplicity, we assume that the Markov chain is irreducible. In this setting, **stability** corresponds to the **positive recurrence** of the Markov chain (Dai & Harrison, 2020; Bramson, 2008). Intuitively, stability means that the backlog of unprocessed prompts does not grow without bound.

Stability Condition. The arrival rate of the queueing system is λ , which is usually easy to estimate. We define the processing rate μ as the maximum expected number of requests that can be fully processed per second under continuous utilization (when the server is never idle). In the queueing theory, the stability condition concerns whether the system remains stable as a function of the relationship between λ and μ .

However, computing μ is highly nontrivial, as it depends on several factors:

1. *KV cache limit M* : A larger memory limit allows more requests to be processed simultaneously.
2. *Input size and output length joint distributions \mathcal{F}_{in-out}* : These distributions directly influence the processing time of each request.
3. *Scheduling and batching algorithm \mathcal{A}* : Different scheduling and batching strategies affect processing efficiency. In this work, we default FCFS with continuous batching, closely aligned with real-world implementations.
4. *Averaged processing time \bar{b}* : The expected time required to process a batch also impacts the overall processing rate.

Thus, we express μ as a function:

$$\mu = f(M, \mathcal{F}_{in-out}, \mathcal{A}, \bar{b}).$$

A key challenge in deriving a closed-form expression for f arises from the dynamic memory usage during LLM inference. Initially, each request’s prompt chunk consumes minimal memory, allowing many requests to be processed together. However, as processing progresses and output tokens are generated, memory usage grows linearly for each request. This causes the number of requests that can be processed simultaneously to decrease over time, leading to significant variability in batch sizes. The interplay between these factors makes it difficult to determine the exact processing rate μ . In the next section, we present a closed-form expression for f and provide a rigorous proof.

4. The Stability and Instability Conditions

In this section, we give rigorous theory on the stability and instability conditions of LLM inference. First, we note that for an arriving request with an input size s , output length o , and the chunk size \hat{s} , the lifetime cumulative memory usage (summed over the entire service of that request) is

$$\begin{aligned} & g(s, o) \\ := & (\hat{s} + 2\hat{s} + \dots + s) + ((s+1) + (s+2) + \dots + (s+o)) \\ = & \frac{(1 + s/\hat{s})s + 2os + (1+o)o}{2}. \end{aligned}$$

To begin with, let us define

$$\mu = \frac{M}{\bar{b} \mathbb{E}_{s,o \sim p} [g(s, o)]} = \frac{M}{\bar{b} \sum_{s,o} g(s, o) p(s, o)}. \quad (1)$$

We show the stability conditions in two steps:

1. We show that $\lambda > \mu$ implies the system is overloaded. (Theorem 4.1)

2. We show that $\lambda < \mu(1 - \delta)$ ensures stability, where $\delta \ll 1$ defined below. (Theorem 4.2).

Theorem 4.1. *If $\lambda > \mu$, then under any scheduling policy, the total number of requests in the system grows to infinity. Namely, the system is overloaded.*

Theorem 4.1 is relatively straightforward. If $\lambda > \mu$, the total memory requirement exceeds the maximum GPU memory capacity. The detailed proof is provided in Appendix A.

Theorem 4.2. *Let $\delta = \frac{\text{ess sup}_{s,o \sim \mathcal{F}_{in-out}} \{s+o\}}{M} \ll 1$. If $\lambda < \mu(1 - \delta)$, then under the work-conserving scheduling and batching policy described in Section 3, the system is stable.*

Proof Sketch. Our stability analysis builds on a Lyapunov argument (Brémaud, 2013), adapted to the unusual memory dynamics of LLM inference. The key idea is to track the *total outstanding memory demand* $V(t)$, defined as the cumulative future KV cache usage required by all active or waiting requests at time t . This quantity grows as new requests arrive, and decreases as the GPU processes batches.

The challenge is that a request’s KV usage is piecewise linear: it grows by chunks in the prompt phase and then by tokens in the decode phase. We overcome this by collapsing each request’s entire future KV trajectory into a single *lifetime memory footprint* $g(s, o)$, and $V(t)$ behaves like “area left to erase.” Per slot (of length \bar{b}), processing with KV utilization U_t reduces V by exactly U_t (we are erasing that much area), independent of whether the consumed work comes from prompt or decode tokens. Under the work-conserving scheduling policies and the memory slack $\delta := \text{ess sup}_{s,o} (s+o)/M$, a large backlog implies a *saturation* property: the batcher can keep utilization $U_t \geq M(1 - \delta)$ throughout the slot without risking overflow (the δ fraction is the headroom needed to accommodate the largest single job).

Meanwhile, new arrivals in a slot contribute an *expected* increase of $\lambda \bar{b} \mathbb{E}[g(s, o)]$ to V . Hence, the conditional one-step drift satisfies

$$\mathbb{E}[V(t+1) - V(t) \mid \text{state at } t] \leq -M(1 - \delta) + \lambda \bar{b} \mathbb{E}[g(s, o)].$$

If $\lambda \bar{b} \mathbb{E}[g(s, o)] < M(1 - \delta)$, i.e., $\lambda < \mu(1 - \delta)$, the drift is strictly negative outside a compact set. By the Foster–Lyapunov criterion, the Markov chain is positive recurrent, so the system is stable. Intuitively, once the backlog is large, the GPU continuously “erases area” at rate $M(1 - \delta)$, while the stochastic inflow adds area at rate $\lambda \bar{b} \mathbb{E}[g(s, o)]$; the former dominates under the stated condition. \square

The detailed proof is provided in Appendix A. In practice, a GPU’s total memory far exceeds the memory needed for a single request. Consequently, Theorems 4.1 and 4.2 together

offer a practical criterion for assessing the stability of LLM inference.

If we have reliable estimates of the arrival rate λ and the service rate μ , this information can not only provide the stability condition for a single-GPU setting, but also guide the flexible provisioning of multiple GPUs. For instance, if system managers aim for a target utilization rate of $\rho = 90\%$, they can estimate the required number of GPUs as approximately $\lambda/(\mu \cdot \rho)$. This approach enables efficient resource allocation, ensuring that the system maintains high throughput while avoiding excessive queuing or memory bottlenecks. Moreover, our results with dynamic estimates of λ and μ can support dynamic scaling strategies, where GPUs are added or removed in response to fluctuating workloads, further improving operational efficiency.

5. Numerical Experiments

In this section, we conduct numerical experiments to validate the accuracy of our theoretical stability condition against real-world measurements. Section 5.1 describes the details of our implementation and hardware environment. Section 5.2 verifies our theory in the single-GPU setting, showing that the error remains within 10%. Section 5.3 demonstrates the robustness and generalizability of our theory in multi-GPU settings, where it still achieves near-perfect predictive power.

5.1. Implementation and Hardware Details

Testbed. Our hardware setup uses eight identical NVIDIA A100 GPUs, with one GPU per replica; we disable intra-model parallelism (tensor parallel size = 1, pipeline stages = 1), so all concurrency comes from replica-level data parallelism across the 8 GPUs. The served LLM is Meta-Llama-3-8B. Each replica runs the vLLM v1 (Kwon et al., 2023) inference engine with chunked prefill enabled: prompts are split into fixed-size segments with $\hat{s} = 512$ to bound per-segment memory use and interleave admission of other requests.

Workload Distributions. We evaluate our stable condition under three distinct prefill-decode (PD) ratio regimes by defining different joint distributions $\mathcal{F}_{\text{in-out}}$ for input (prefill) and output (decode) token lengths:

1. **PD Ratio 1:1:** Prefill (input length) and decode (output length) are independently sampled from Uniform(10, 1600) respectively.
2. **PD Ratio 2:1:** Prefill and decode are independently sampled from Uniform(10, 2133) and Uniform(10, 1066) respectively.
3. **PD Ratio 1:2:** Prefill and decode are independently sampled from Uniform(10, 1066) and

Uniform(10, 2133) respectively.

Here, we control the decode length per request using the functionality in vLLM v1, which allows setting upper and lower bounds. For instance, in the 1:1 PD ratio setup, we sample a prefill length and set both the lower and upper decoding bounds to this value, thereby enforcing the desired ratio.

Parameter Selection. The memory capacity parameter M is set to 131,000 tokens, based on the observed maximum capacity of the GPU memory in our testbed.

To determine the characteristic processing time \bar{b} , we adopted a data-driven approach. Empirical analysis of real traces Figure 5 in Appendix B revealed that the median batch processing time is a robust estimator, aligning closely with the 90th percentile in many cases. For each experimental setup, we simulated 10,000 jobs from the respective distribution to form a training dataset. We then computed the median processing time of these batches to obtain \bar{b} for that specific workload:

- **PD Ratio 1:1:** $\bar{b} = 0.0372\text{s}$;
- **PD Ratio 2:1:** $\bar{b} = 0.0430\text{s}$;
- **PD Ratio 1:2:** $\bar{b} = 0.0337\text{s}$.

5.2. Single-GPU Results

We evaluate the accuracy of our theoretical stable processing rate, μ_{theory} (from Equation equation 1), against empirically measured values from the GPU, μ_{gpu} . To ensure our measurement captures the system’s steady-state behavior, we calculate the empirical processing rate μ_{gpu} by excluding the first and last 1,000 requests, which may be affected by initial warm-up and termination phases. The measurement time interval is defined from the arrival time of the 1,001st request to one of the last 1,000th request to make sure that requests that completed during the termination phases are not included as by including these requests, the latency statistics can be artificially improved. The empirical rate is then computed as the total number of processed requests within this interval divided by its duration. Therefore, μ_{gpu} can be interpreted as the averaged number of requests can be completed by the real GPU within 1 second. To quantify the accuracy of our model, we use the Gap Absolute Percentage (GAP):

$$\text{GAP} = \frac{|\mu_{\text{theory}} - \mu_{\text{gpu}}|}{\mu_{\text{gpu}}}$$

In Table 1, all values converge when the arriving rate $\lambda \geq 5$. As shown in the table, the theoretical processing rates derived from Equation equation 1 closely align with the empirically measured rates from the GPU hardware. Across

Table 1. Stable Condition of Single GPU under Different PD Ratios.

P/D Ratio	μ_{gpu}	μ^{theory}	GAP
1 : 1	3.387	3.263	3.66%
2 : 1	3.650	3.956	8.38%
1 : 2	2.969	2.902	2.25%
Mixed 2 : 1 \rightarrow 1 : 2	3.137	3.385	7.90%

all three fixed PD ratio settings (1:1, 2:1, and 1:2), the GAP remains below 10%, demonstrating the high accuracy of our model. We also evaluate a time-varying request-size distribution. The trace consists of two consecutive segments: the first half of requests follows the PD 2:1 distribution, and the second half follows the PD 1:2 distribution. For a trace in which a fraction q_ℓ of requests follows distribution F_ℓ , the predicted long-run processing rate is

$$\mu_{\text{mix}} = \frac{M}{\sum_\ell q_\ell \bar{b}_\ell \mathbb{E}_{F_\ell}[g(s, o)]} = \left(\sum_\ell \frac{q_\ell}{\mu_\ell} \right)^{-1}.$$

For $q_1 = q_2 = 1/2$, this gives $\mu^{\text{theory}} = 3.385$, while the measured rate is $\mu_{\text{gpu}} = 3.137$, yielding a 7.90% gap. This remains within the empirical error range observed in the stationary workloads, suggesting that the formula remains a useful long-run capacity predictor under piecewise-stationary workload distributions. Overall, these results are practically significant, as they enable reliable estimation of the required number of GPUs during system deployment to ensure stability under expected workloads.

We now examine the system dynamics under a 1:1 P/D ratio by varying the arrival rate λ . Figure 4b plots the evolution of queue length over time for arrival rates of $\lambda = 5, 20$, and 50 requests per second. The queue length increases approximately linearly in all cases, indicating the system overload where the arrival rate exceeds the service rate. For arrival rates of $\lambda = 1, 3$, the queue length is usually upper bounded by 5, indicating the system is stable where the service rate exceeds the arrival rate.

Furthermore, we plot the CDF of the per-request waiting time (i.e., the delay between arrival and the start of processing) in Appendix B, Figure 6, and the findings are consistent to Figure 2.

Real Dataset Experiment To validate our findings beyond simulations with fixed prefill/decode (P/D) ratios, we evaluate our model on the LongBench v2 dataset (Bai et al., 2025), which features highly variable and dependent P/D lengths. This benchmark contains 503 complex, long-context questions, providing a realistic distribution of request complexities. Figure 3 visualizes this relationship, showing the marginal probability densities of prefill

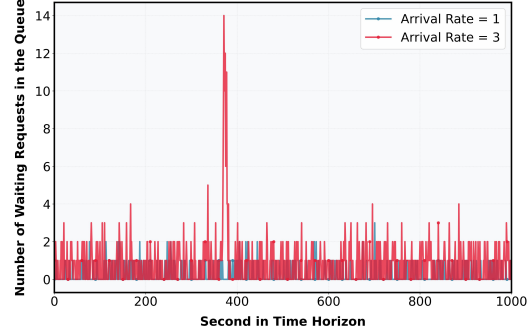
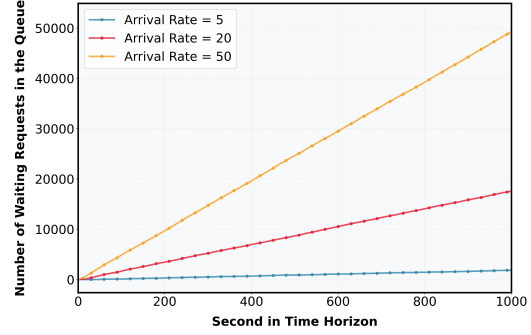

 (a) $\lambda = 1, 3$

 (b) $\lambda = 5, 20, 50$

Figure 2. Number of waiting requests in the queue under different arrival rates.

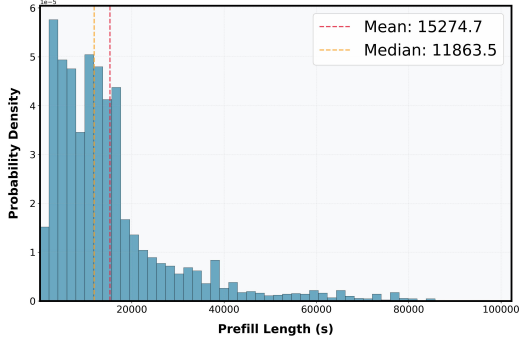
(s) and decode (o) lengths, alongside their joint cumulative distribution function. The dataset is publicly accessible at <https://longbench2.github.io/>.

In our experiment setup, we partition the dataset randomly, using 80% to compute the joint probability density function $p(s, o)$ and to estimate the mean batch processing time \bar{b} via a 10% trimmed average (to mitigate the effect of heavy-tailed outliers). The remaining 20% is used for testing under a load of 20 queries per second (qps).

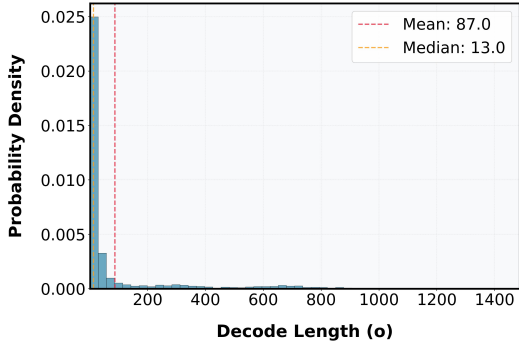
Table 2. Stable Condition of Single GPU under the LongBench v2 dataset.

μ_{gpu}	μ^{theory}	GAP
0.610	0.561	8.03%

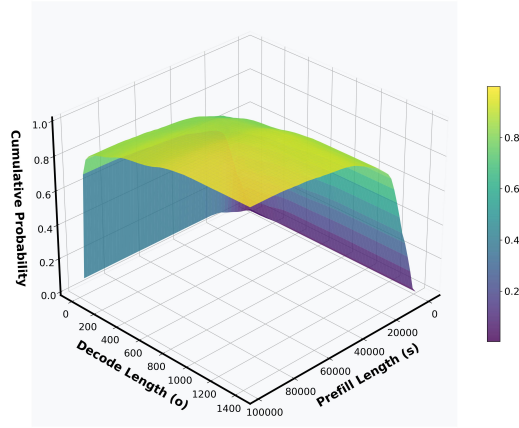
As shown in Table 2, the theoretical stable condition μ^{theory} closely matches the empirically observed condition μ_{gpu} , with an error of only 8.03%. This strong agreement underscores the importance of modeling the full joint distribution $p(s, o)$ rather than relying on simplified expectations, as it effectively captures the complex dependencies and high variance between prefill and decode lengths inherent in real-world workloads.



(a) Marginal probability density function of prefill length (s)



(b) Marginal probability density function of decode length (o)

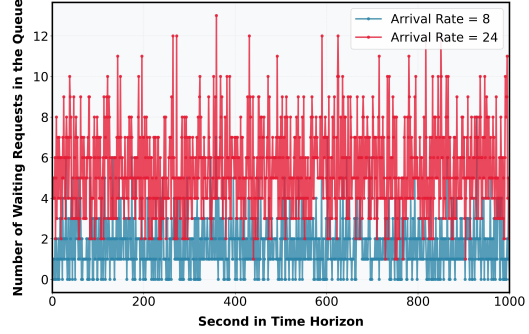


(c) Joint cumulative density function of prefill length and decode length (s, o)

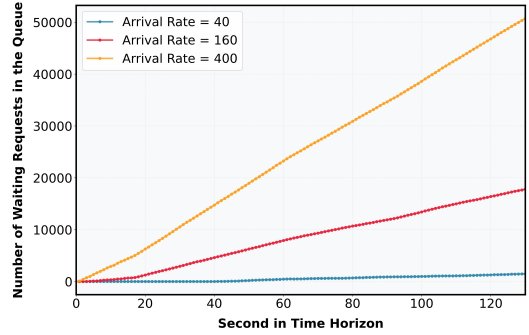
Figure 3. Joint PDF and CDF of the LongBench v2 dataset.

5.3. Eight-GPU Results

Next, we conduct 8-GPU experiments to compare the real processing rate and the theoretical rate multiplies by 8, i.e. $8\mu_{\text{theory}}$, to see whether our approximation still is accurate or not in the cluster deployment. In our 8-GPU configuration, we deploy eight identical single-GPU replicas (NVIDIA A100) serving Meta-Llama-3-8B with no intra-model parallelism. Incoming requests are statelessly load-balanced



(a) $\lambda = 8, 24$



(b) $\lambda = 40, 160, 400$

Figure 4. Number of total waiting requests among 8 GPUs in the queue under different arrival rates.

across replicas using the round robin over 56,000 requests. The PD ratio is 1 : 1 and again the prefill and decode are independently sampled from Uniform(10,1600).

Table 3. Stable Condition of 8 Parallel GPUs.

P/D Ratio	μ_{gpu}	μ_{theory}	GAP
1 : 1	26.710	25.808	3.38%

As shown in Table 4, our theoretical model achieves strong convergence with empirical results for arrival rates $\lambda \geq 40$, corresponding to a per-GPU rate of ≥ 5 requests per second. The gap between the empirical processing rate μ_{gpu} and the theoretical rate μ_{theory} is only 3.38%, demonstrating the model’s high accuracy. This validates the practical utility of our approach for capacity planning: it provides an accurate lower bound on the number of GPUs required to ensure system stability—defined as a regime where no GPU is idle and the queue length remains bounded—for a given workload distribution.

Again, in Figure 4, we visualize the total queue length of 8 GPUs during processing time horizon. The insights is similar to the ones for single GPU in Figure 2: while the rates $\lambda = 40, 160, 400$ are greater than the service rate $\mu_{\text{gpu}} = 26.710$, the queue length linearly grows and the

system is overloaded. For the rates $\lambda = 8, 24$, which are smaller than the service rate, the queue length is upper bounded by 13, indicating the system is stable.

6. Conclusion and Discussion

This paper presents a queueing-theoretic model for LLM inference, characterizing stable GPU operation by accounting for computational demand and KV cache memory constraints. We derived the stability condition and critical processing rate μ for a single GPU, validated empirically on a real GPU testbed with less than 10% discrepancy between theoretical and measured service rates across various workloads. This provides a foundation for capacity planning, enabling system designers to estimate the minimum number of GPUs, $\lceil \lambda/\mu \rceil$, using the request arrival rate λ and per-GPU service rate μ , ensuring efficient resource provisioning to avoid over-provisioning (idle GPUs) or under-provisioning (missed service-level objectives).

Scope and architectural extensions. Our experiments focus on single-GPU replicas and data-parallel multi-GPU deployment. Tensor parallelism can be incorporated as a parameter-level extension by treating a TP group as one logical worker: the queueing structure and the formula for μ remain unchanged after replacing M and \bar{b} by their TP-specific effective values. These quantities should be measured empirically, since communication overheads such as all-reduce prevent linear scaling in the TP degree. By contrast, pipeline parallelism and prefill-decode disaggregation change the queueing topology into tandem or networked queues with separate memory constraints and inter-stage transfers. Deriving closed-form stability conditions for these architectures is an important direction for future work.

Impact Statement

This work provides a principled foundation for designing and operating large-scale LLM inference systems under realistic memory constraints. Its potential impact lies in enabling practitioners to quantitatively balance capacity and demand, thereby reducing both over-provisioning—which wastes energy and capital—and under-provisioning, which degrades user experience and system reliability. As LLMs become critical infrastructure across education, healthcare, and industry, such principled capacity-planning tools are essential for making AI services efficient, sustainable, and dependable at scale.

References

Agrawal, A., Panwar, A., Mohan, J., Kwatra, N., Gulavani, B. S., and Ramjee, R. Sarathi: Efficient LLM inference by piggybacking decodes with chunked prefills. *arXiv preprint arXiv:2308.16369*, 2023.

- Agrawal, A., Kedia, N., Panwar, A., Mohan, J., Kwatra, N., Gulavani, B. S., Tumanov, A., and Ramjee, R. Taming throughput-latency tradeoff in LLM inference with Sarathi-Serve. *arXiv preprint arXiv:2403.02310*, 2024.
- An, C., Huang, F., Zhang, J., Gong, S., Qiu, X., Zhou, C., and Kong, L. Training-free long-context scaling of large language models. *arXiv preprint arXiv:2402.17463*, 2024.
- Ao, R., Luo, G., Simchi-Levi, D., and Wang, X. Optimizing llm inference: Fluid-guided online scheduling with memory constraints. *arXiv preprint arXiv:2504.11320*, 2025.
- Bai, Y., Tu, S., Zhang, J., Peng, H., Wang, X., Lv, X., Cao, S., Xu, J., Hou, L., Dong, Y., et al. Longbench v2: Towards deeper understanding and reasoning on realistic long-context multitasks. In *Proceedings of the 63rd Annual Meeting of the Association for Computational Linguistics (Volume 1: Long Papers)*, pp. 3639–3664, 2025.
- Bramson, M. *Stability of queueing networks: École d'Été de Probabilités de Saint-Flour XXXVI-2006*. Springer, 2008.
- Brémaud, P. *Markov chains: Gibbs fields, Monte Carlo simulation, and queues*, volume 31. Springer Science & Business Media, 2013.
- Brown, T., Mann, B., Ryder, N., Subbiah, M., Kaplan, J. D., Dhariwal, P., Neelakantan, A., Shyam, P., Sastry, G., Askell, A., et al. Language models are few-shot learners. *Advances in neural information processing systems*, 33: 1877–1901, 2020.
- Chen, Z., Ye, Y., and Zhou, Z. Adaptively robust llm inference optimization under prediction uncertainty. *arXiv preprint arXiv:2508.14544*, 2025.
- Chen, Z., Bu, T., Song, C., Lu, X., Ye, Y., and Zhou, Z. A universal load balancing principle and its application to large language model serving. *arXiv preprint arXiv:2601.17855*, 2026.
- Chowdhery, A., Narang, S., Devlin, J., Bosma, M., Mishra, G., Roberts, A., Barham, P., Chung, H. W., Sutton, C., Gehrmann, S., et al. Palm: Scaling language modeling with pathways. *Journal of Machine Learning Research*, 24(240):1–113, 2023.
- Coffman, E. and Stolyar, A. L. Bandwidth packing. *Algorithmica*, 29(1):70–88, 2001.
- Dai, J. and Harrison, J. M. *Processing networks: fluid models and stability*. Cambridge University Press, 2020.

- Gamarnik, D. Stochastic bandwidth packing process: stability conditions via lyapunov function technique. *Queueing systems*, 48(3):339–363, 2004.
- Ghaderi, J., Zhong, Y., and Srikant, R. Asymptotic optimality of bestfit for stochastic bin packing. *ACM SIGMETRICS Performance Evaluation Review*, 42(2):64–66, 2014.
- GilPress. ChatGPT users statistics. WhatsTheBigData, 2024. URL https://whatsthebigdata.com/chatgpt-users/#google_vignette.
- GitHub. GitHub copilot. <https://github.com/features/copilot>, 2021.
- Gordon, C. ChatGPT and Generative AI innovations are creating sustainability havoc. *Forbes*, 2024. URL <https://www.forbes.com/sites/cindygordon/2024/03/12/chatgpt-and-generative-ai-innovations-are-creating-sustainability-havoc>.
- Guldogan, O., Kunde, J., Lee, K., and Pedarsani, R. Multi-bin batching for increasing llm inference throughput. *arXiv preprint arXiv:2412.04504*, 2024.
- Gupta, V. and Radovanovic, A. Lagrangian-based online stochastic bin packing. *ACM SIGMETRICS Performance Evaluation Review*, 43(1):467–468, 2015.
- Hoffmann, J., Borgeaud, S., Mensch, A., Buchatskaya, E., Cai, T., Rutherford, E., Casas, D. d. L., Hendricks, L. A., Welbl, J., Clark, A., et al. Training compute-optimal large language models. *arXiv preprint arXiv:2203.15556*, 2022.
- Huang, C., Tang, Z., Hu, S., Jiang, R., Zheng, X., Ge, D., Wang, B., and Wang, Z. Orlm: A customizable framework in training large models for automated optimization modeling. *Operations Research*, 2025.
- Jaillet, P., Jiang, J., Mellou, K., Molinaro, M., Podimata, C., and Zhou, Z. Online scheduling for llm inference with kv cache constraints. *arXiv preprint arXiv:2502.07115*, 2025.
- Kaplan, J., McCandlish, S., Henighan, T., Brown, T. B., Chess, B., Child, R., Gray, S., Radford, A., Wu, J., and Amodei, D. Scaling laws for neural language models. *arXiv preprint arXiv:2001.08361*, 2020.
- Kwon, W., Li, Z., Zhuang, S., Sheng, Y., Zheng, L., Yu, C. H., Gonzalez, J., Zhang, H., and Stoica, I. Efficient memory management for large language model serving with PagedAttention. In *Proceedings of the 29th Symposium on Operating Systems Principles*, pp. 611–626, 2023.
- Li, Y., Dai, J., and Peng, T. Throughput-optimal scheduling algorithms for llm inference and ai agents. *arXiv preprint arXiv:2504.07347*, 2025.
- Maguluri, S. T., Srikant, R., and Ying, L. Stochastic models of load balancing and scheduling in cloud computing clusters. In *2012 Proceedings IEEE Infocom*, pp. 702–710. IEEE, 2012.
- Mitzenmacher, M. and Shahout, R. Queueing, predictions, and llms: Challenges and open problems. *arXiv preprint arXiv:2503.07545*, 2025.
- OpenAI. ChatGPT. <https://chat.openai.com>, 2019.
- OpenAI. GPT-4 technical report. arxiv 2303.08774. *View in Article*, 2(5), 2023.
- Pope, R., Douglas, S., Chowdhery, A., Devlin, J., Bradbury, J., Heek, J., Xiao, K., Agrawal, S., and Dean, J. Efficiently scaling transformer inference. *Proceedings of Machine Learning and Systems*, 5:606–624, 2023.
- Ratner, N., Levine, Y., Belinkov, Y., Ram, O., Magar, I., Abend, O., Karpas, E., Shashua, A., Leyton-Brown, K., and Shoham, Y. Parallel context windows for large language models. *arXiv preprint arXiv:2212.10947*, 2022.
- Stolyar, A. L. An infinite server system with general packing constraints. *Operations Research*, 61(5):1200–1217, 2013.
- Stolyar, A. L. and Zhong, Y. A large-scale service system with packing constraints: Minimizing the number of occupied servers. *ACM SIGMETRICS Performance Evaluation Review*, 41(1):41–52, 2013.
- Stolyar, A. L. and Zhong, Y. Asymptotic optimality of a greedy randomized algorithm in a large-scale service system with general packing constraints. *Queueing Systems*, 79(2):117–143, 2015.
- Wang, M., Ye, Y., and Zhou, Z. Llm serving optimization with variable prefill and decode lengths. *arXiv preprint arXiv:2508.06133*, 2025.
- Wei, J., Tay, Y., Bommasani, R., Raffel, C., Zoph, B., Borgeaud, S., Yogatama, D., Bosma, M., Zhou, D., Metzler, D., et al. Emergent abilities of large language models. *arXiv preprint arXiv:2206.07682*, 2022.
- Wu, B., Zhong, Y., Zhang, Z., Liu, S., Liu, F., Sun, Y., Huang, G., Liu, X., and Jin, X. Fast distributed inference serving for large language models. *arXiv preprint arXiv:2305.05920*, 2023.

Yang, Y., Jiao, L., and Xu, Y. A queueing theoretic perspective on low-latency llm inference with variable token length. In *2024 22nd International Symposium on Modeling and Optimization in Mobile, Ad Hoc, and Wireless Networks (WiOpt)*, pp. 273–280. IEEE, 2024.

Yen, H., Gao, T., and Chen, D. Long-context language modeling with parallel context encoding. *arXiv preprint arXiv:2402.16617*, 2024.

A. Proofs of Theorem 4.1 and 4.2

Proof of Theorems 4.1. We will show that the total outstanding memory needed in the GPU (including the chunks in the prompt phase) diverges to infinity.

For each arriving request with an input size s , output length o , and the chunk size \hat{s} , the cumulative memory usage in the GPU (summed over the entire service of that request) is

$$g(s, o) = (\hat{s} + 2\hat{s} + \dots + s) + ((s+1) + (s+2) + \dots + (s+o)) = \frac{(1 + s/\hat{s})s + 2os + (1+o)o}{2}.$$

As the p.m.f. of joint distribution of arrival is $p(s, o)$, then the expected cumulative memory usage is

$$\mathbb{E}_{s, o \sim p(s, o)} \left[\frac{(1 + s/\hat{s})s + 2os + (1+o)o}{2} \right]$$

Given that the arrival process has mean $\lambda \bar{b}$ in each slot, the expected total memory demand over the time period $[0, T]$ (assuming T is a multiple of \bar{b}) is

$$\lambda T \mathbb{E}_{s, o \sim p(s, o)} \left[\frac{(1 + s/\hat{s})s + 2os + (1+o)o}{2} \right].$$

By the strong law of large numbers for i.i.d. arrivals, we have

$$\frac{1}{T} \sum_{i=1}^{N(T)} g(s_i, o_i) \rightarrow \lambda \mathbb{E}_{s, o \sim p(s, o)} \left[\frac{(1 + s/\hat{s})s + 2os + (1+o)o}{2} \right], \text{ almost surely,} \quad (2)$$

where $N(T)$ denotes the number of arrivals up to time T , and s_i and o_i are the prompt length and decode length of the i -th arrival, respectively.

Now, we turn to the service side. As each batch takes \bar{b} seconds, we can take $\frac{1}{\bar{b}}$ batches per second. Moreover, at any instant in time, the memory usage cannot exceed M . This implies that the maximum total memory supply over the time period $[0, T]$ is:

$$T \times M \text{ (units of memory)} \times \frac{1}{\bar{b}} \text{ (batches/second)} = \frac{TM}{\bar{b}}.$$

Therefore, if $\lambda > \mu$, we have

$$\lambda T \mathbb{E}_{s, o \sim p(s, o)} \left[\frac{(1 + s/\hat{s})s + 2os + (1+o)o}{2} \right] - \frac{TM}{\bar{b}} \rightarrow +\infty, \text{ as } T \rightarrow +\infty.$$

Hence, by combining with Equation (2), the total number of unprocessed tokens diverges to infinity almost surely. \square

Proof of Theorem 4.2. We use a Lyapunov argument to show that, for large values of the Lyapunov function, the expected net change in the function is negative whenever $\lambda < \mu(1 - \delta)$. By the Foster–Lyapunov theorem (Brémaud, 2013, Section 5.1), this implies positive recurrence, and hence the system is stable. In the following derivation, one step corresponds to a duration of \bar{b} time.

Let $V(t)$ denote the total outstanding memory demand (including the chunks in the prompt phase) in the system at time t . Concretely, if a request is partially completed, only its remaining memory demand contributes to $V(t)$. For a prompt $i \in S^{(t)}$ with the index of the prefill chunk $c_i^t > 0$, the remaining memory demand is given by

$$v_i(t) := \begin{cases} ((c_i^t + 1)\hat{s} + \dots + s_i + (s_i + 1)) + (s_i + 2) + \dots + (s_i + o_i), & \text{if } c_i^t < s_i/\hat{s}, \\ (s_i + d_i^t + 1) + \dots + (s_i + o_i), & \text{if } c_i^t \geq s_i/\hat{s}, \end{cases}$$

which can be simplified to

$$v_i(t) := \begin{cases} \frac{1}{2}(c_i^t \hat{s} + s)(s/\hat{s} - c_i^t + 1) + o_i s_i + \frac{(1+o_i)o_i}{2}, & \text{if } c_i^t < s_i/\hat{s}, \\ s_i(o_i - d_i^t + 1) + \frac{(o_i - d_i^t + 1)(o_i + d_i^t)}{2}, & \text{if } c_i^t \geq s_i/\hat{s}. \end{cases}$$

On the other hand, if a request has arrived but is still waiting (i.e., not yet started), namely $i \in W^{(t)}$, then its outstanding memory demand is

$$v_i(t) := g(s_i, o_i) = \frac{(1+s_i/\hat{s})s_i+2o_i s_i+(1+o_i)o_i}{2}.$$

If a prompt has finished, it no longer contributes. Therefore, the total outstanding memory demand is

$$V(t) = \sum_{i \in S^{(t)} \cup W^{(t)}} v_i(t).$$

We now show that $V(t)$ is a valid Lyapunov function. Specifically, we consider a sufficiently large constant

$$K = \left(\sup_{s, o \sim p(s, o)} g(s, o) \right) M,$$

which corresponds to the situation where there are at least M prompts either waiting in the queue or being processed by the system.

We will establish that

$$\mathbb{E}[V(t+1) | S^{(t)} \cup W^{(t)}; \{\{c_i(t), d_i(t)\}, i \in S^{(t)} \cup W^{(t)}\}] \leq V(t) - \varepsilon, \quad \text{whenever } V(t) > K, \quad (3)$$

for some $\varepsilon > 0$.

We first decompose $V(t+1)$. Between time t and $t+1$, some fraction of the old $W(t)$ (the tokens present at time t) is completed, and a random number of new requests arrive. Hence, we can write:

$$V(t+1) = \underbrace{V(t) - (\# \text{ old memory fulfilled})}_{\text{old backlog that remains}} + (\text{memory demand from newly arrived requests}). \quad (4)$$

If $V(t) > \sup_{s, o \sim p(s, o)} g(s, o)M$, then there are more than M unfinished requests in $S^{(t)} \cup W^{(t)}$, since each request contributes at most $\sup_{s, o \sim p(s, o)} g(s, o)$ to $V(t)$. Under our work-conserving scheduling policy, the batching rule is maximal: it keeps adding feasible old requests until no remaining old request can be added without violating the memory constraint. Moreover, the next-step memory requirement of any single request is at most

$$\text{ess sup}_{s, o} (s + o) = \delta M.$$

Therefore, if the total amount of old memory fulfilled in the next slot were strictly smaller than $M(1 - \delta)$, then the remaining memory capacity would be strictly larger than δM . In that case, at least one remaining old request could still be admitted, contradicting the maximality of the batching rule. Hence,

$$(\# \text{ old memory fulfilled}) \geq M(1 - \delta).$$

On the other hand, we have

$$\mathbb{E}[\text{memory demand from newly arrived requests}] = \lambda \bar{b} \mathbb{E}_{s, 0 \sim p(s, o)} [g(s, o)].$$

Therefore, we have

$$\begin{aligned} \mathbb{E}[V(t+1) | S^{(t)} \cup W^{(t)}; \{a_i(t), i \in S^{(t)} \cup W^{(t)}\}] &< V(t) - M(1 - \delta) + \lambda \bar{b} \mathbb{E}_{s, 0 \sim p(s, o)} [g(s, o)] \\ &= V(t) - (\mu(1 - \delta) - \lambda) \bar{b} \mathbb{E}_{s, 0 \sim p(s, o)} [g(s, o)]. \end{aligned}$$

Due to $\lambda < \mu(1 - \delta)$ and $\mathbb{E}_{s, 0 \sim p(s, o)} [g(s, o)] > 0$, we can choose

$$\varepsilon = (\mu(1 - \delta) - \lambda) \bar{b} \mathbb{E}_{s, 0 \sim p(s, o)} [g(s, o)],$$

which proves (3). □

B. Additional Numerical Plots

B.1. Batch Processing Time Plot in Real Traces

Figure 5 presents the cumulative distribution function (CDF) of batch execution times across several real-world traces. The subfigures are organized by workload: the first row corresponds to a prefill-decode (PD) ratio of 2:1, and the second row to a ratio of 4:1. The first column represents a low arrival rate (5 requests/second), while the second column represents a higher rate (20 requests/second). For context, Figure 1 in the main text shows the case for a 1:1 PD ratio at 5 requests/second. We observe that the batch execution time is nearly identical for different arrival rates λ . However, as the PD ratio increases, we note a corresponding increase in the disparity of execution times. This variability presents a promising direction for future modeling efforts.

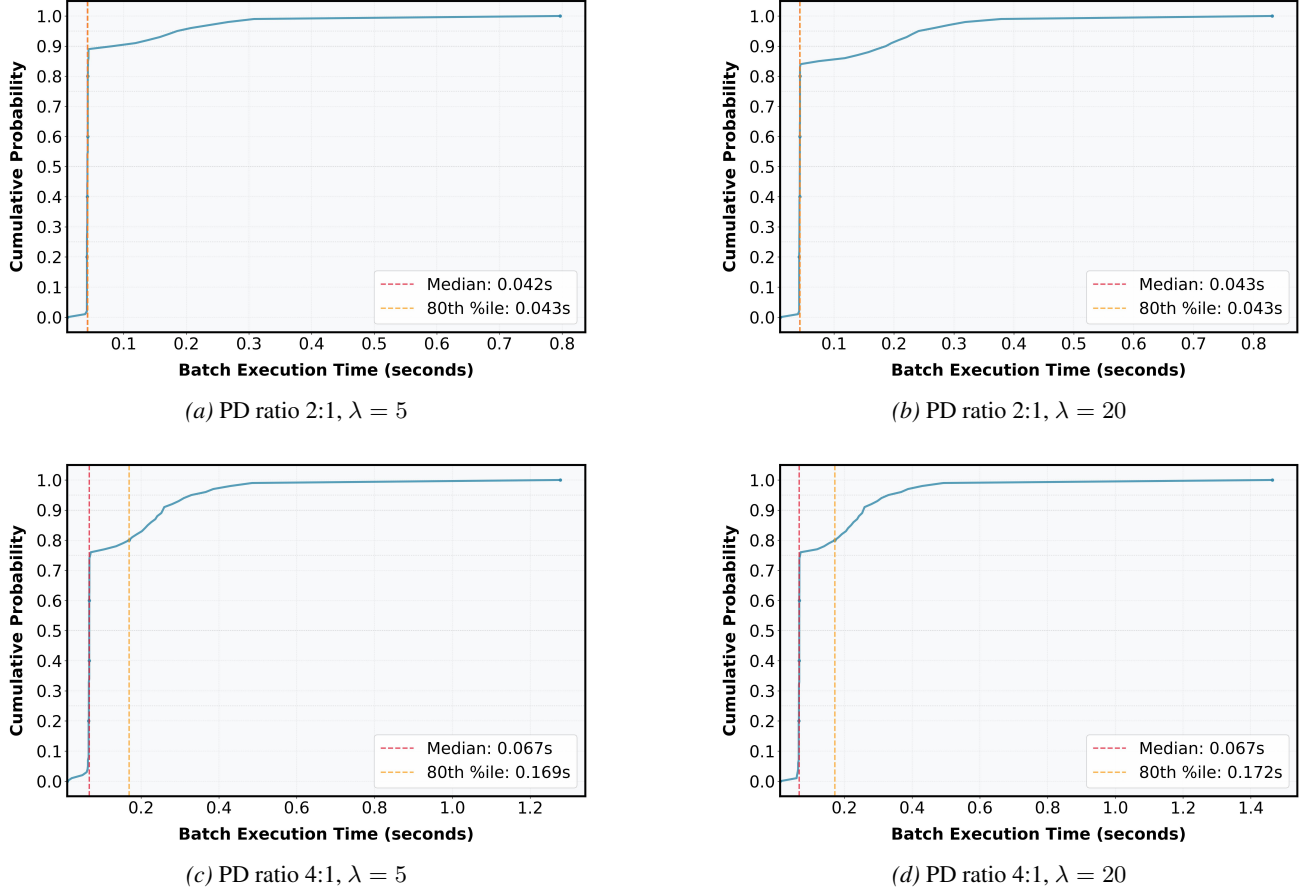


Figure 5. Cumulative Distribution Function (CDF) for Batch Execution Time under different PD ratios and arrival rates.

B.2. CDF for Waiting Time of Each Request

The near-linear growth of the CDF under $\lambda = 4, 5$ indicates an overloaded system. This provides further evidence for the system instability at this arrival rate and explains why the empirical processing rate μ_{gpu} converges for $\lambda \geq 5$. Moreover, under $\lambda = 2$, we can find the system is stable, and almost no request waits in the queue. Finally, for a special case $\lambda = 3.387 = \mu_{\text{gpu}}$, which is called as an unstable system in queueing theory, the growth of CDF indicates a linear trend but a non-smooth shape. This is also consistent with the theory of queueing for the unstable system.

C. Stable Condition under an 8:1 P/D Ratio

This section presents a complementary numerical experiment under a more extreme workload compared to those in Section 5.2. While Section 5.2 evaluated P/D ratios of 1:1, 2:1, and 1:2—where batch processing times were largely consistent—we

Queueing-Theoretic Stability for LLM Inference

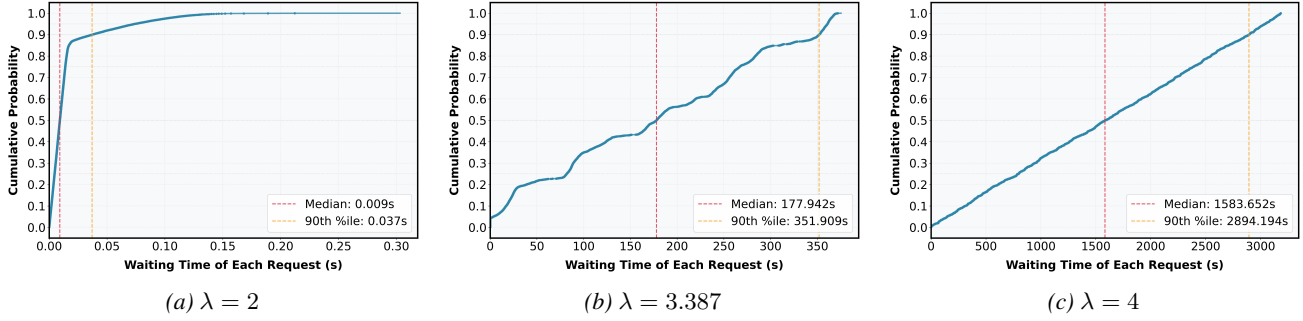


Figure 6. Cumulative Distribution Function (CDF) for Waiting Time of Each Request.

observe that as the P/D ratio increases, the tail of the processing time distribution becomes significantly heavier, as shown in Figure 7.

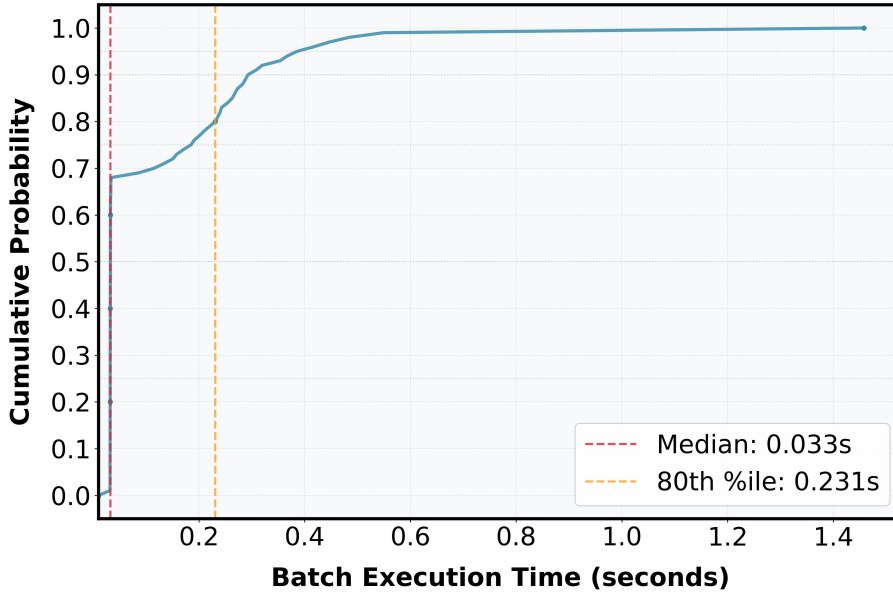


Figure 7. Cumulative Distribution Function (CDF) for Batch Execution Time under an 8:1 P/D ratio.

Figure 7 shows that while the first 70% of batches have nearly identical processing times, the remaining 30% exhibit a heavy tail. In this regime, neither the median nor the mean is a robust estimator for \bar{b} : the median ignores the heavy tail, while the mean is dominated by it.

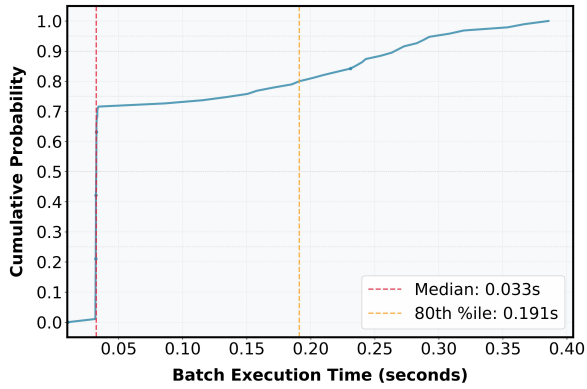
A standard statistical approach for heavy-tailed distributions is the **trimmed mean**, which discards a top percentage $x\%$ of the data (treating them as outliers) and calculates the mean of the remainder. Common choices for x are 5 or 10. Figure 8 shows the CDF of the trimmed batch processing time. Table 4 compares the results using these two trimmed-mean estimators for \bar{b} .

Table 4. Stable Condition of a Single GPU under an 8:1 P/D Ratio.

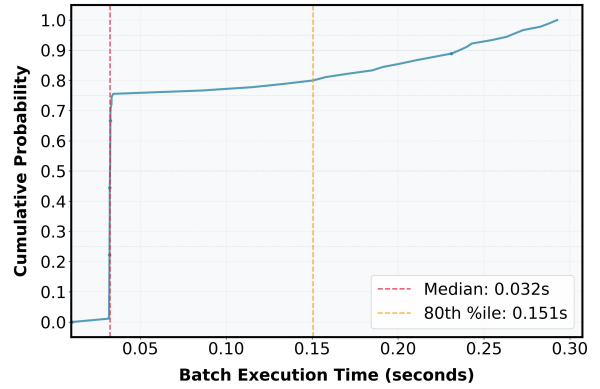
$x\%$	Trimmed Mean	μ_{gpu}	μ_{theory}	GAP
5%		5.470	4.977	9.0%
10%		5.470	5.862	7.2%

The results in Table 4 demonstrate that even under the extreme heavy-tailed distribution of an 8:1 P/D ratio, our theoretical model remains accurate. Using a robust estimator for \bar{b} yields a predicted service rate μ_{theory} that is close to the empirically

measured μ_{gpu} , with gaps of only 9.0% and 7.2%. This highlights the robustness of our theoretical approach when combined with appropriate statistical estimation techniques.



(a) 5% Trimmed Batch Execution Time



(b) 10% Trimmed Batch Execution Time

Figure 8. Trimmed Cumulative Distribution Function (CDF) for Batch Execution Time.